JOURNAL OF CATALYSIS 70, 53–71 (1981)

Oxidation of Silica-Supported Pt, Ir, and Pt/Ir Catalysts

K. FOGER AND H. JAEGER

CSIRO, Division of Materials Science, University of Melbourne, Parkville, Victoria, Australia

Received August 20, 1980; revised January 5, 1981

Pt and Ir impregnated alone or together on SiO_2, Aerosil (Degussa), have been examined with X-ray diffraction, transmission electron microscopy, and temperature-programmed reduction as prepared and after heating in O_2 or in 1% O_2 in He at temperatures (T_{ox}) in the range 100–700°C. Mostly single-phase Pt/Ir alloy particles are formed only when the ratio of Pt to Ir is close to 50/50. The surface composition of such particles is about Pt 73%, Ir 27%. On heating, no oxide is detected with Pt but the particle size increases. With Ir and Pt/Ir (50/50), a surface oxide, Ir_xO, is formed if $T_{ox} < 300$°C, but IrO_2 as thin blades or sheets grows out from metal particles if $T_{ox} > 300$°C. Pure Ir is completely oxidized at $T_{ox} = 550$°C but in Pt/Ir(50/50) alloy only 65% of the Ir is oxidized at $T_{ox} = 700$°C when most oxide crystals have been separated from residual metal particles by gas phase transport of IrO_2. The reduction of oxide is autocatalytic; once metal particles have been nucleated, atomic hydrogen is produced which nucleates further metal particles on the adjacent oxide. Agglomerates of heavily faulted Ir metal particles are formed on reduction. Thus oxidation and reduction appreciably diminish the metal surface area and destroy the single-phase alloy.

INTRODUCTION

Platinum metal supported on various oxides has been used traditionally as a reforming catalyst in the petroleum industry. The search for more selective catalysts initiated the development of supported bimetallic catalysts, based mainly on the Pt/Re system. More recently, it has been claimed (*1*) that Pt/Ir alloy catalysts exhibit higher selectivity and activity and a lower tendency to "coke" formation than Pt/Re catalysts. However, under the conditions of elevated temperatures and oxidizing atmospheres needed to burn off the "coke," Ir forms oxides of significant volatility. From X-ray diffraction and Mössbauer spectroscopy it has been concluded that these oxides form large grains separate from the original alloy particles. (*2a,b*). Thus Ir is lost from the alloy particles and the catalysts lose their desirable properties. As a practical measure it has been suggested that after the carbon has been burned off, catalysts should be treated with halogen-containing compounds to redisperse Pt and Ir. It is claimed that this procedure prevents large Ir clusters and restores the initial catalytic activity (*3*).

To understand how supported catalysts change during operation and regeneration, it is important to examine the morphology, distribution, size, and structure of metal particles after different exposures. Studies on the rate of oxidation of bulk specimens of Ir and Pt and the thermodynamic stability of the resulting oxides have been reported before (*4*). Work on the stability of Pt and Ir particles on various supports has also been carried out (*5*) but a systematic comparison of the oxidation behavior of Pt, Ir, and Pt/Ir alloy particles has not been reported before. We have therefore exposed such particles to various reaction and oxidation conditions and have then examined them with temperature-programmed reduction (TPR), X-ray diffraction (XRD), transmission electron microscopy (TEM), and selected-area diffraction (SAED). Although γ-Al_2O_3 is the common support in reforming catalysts, we chose SiO_2 as support because exploratory experiments showed that the 222 γ-Al_2O_3 peak prevented us from observing details in the 111

0021-9517/81/070053-19$02.00/0

metal peaks when the metal loadings of the catalysts were low.

EXPERIMENTAL

Catalyst Preparation

In preparing the catalysts (Table 1) a slurry of aqueous H_2PtCl_6 and/or H_2IrCl_6 with Aerosil (Degussa) was dried in air at 100°C and then heated for 15 hr in H_2 at 400°C.

Catalysis

Catalysts 1, 2, and 3 were tested for the conversion of *n*-heptane in a flow apparatus, as described previously (*6*). The H_2 to HC ratio was 20 to 1 and the space velocity (WHSV) was constant at 1 hr^{-1}. These conditions are not suitable if the initial product distributions and thus the selectivity of catalysts is of interest, but they readily enable one to demonstrate changes in surface composition and the presence or absence of separate Ir particles in catalysts.

Oxidation–TPR

Catalysts were heated at selected temperatures (T_{ox}) in the range 100–700°C for 1 hr either *in situ* in 1% O_2 in He, or externally in a flow apparatus (30 cm^3 STP min^{-1} O_2) or in a static system in air. They were then flushed with N_2 at the selected temperature for 30 min and also while they cooled to room temperature. Subsequently the carrier gas was switched to 3% H_2 in N_2 and after obtaining a stable baseline on the chart recorder connected to the Carle Thermistor gas chromatograph used as detector, the temperature was increased at a rate of 5°C min^{-1} in the range 25 to 400°C. Usually a fresh sample of catalyst was used for an oxidation–TPR cycle, but some samples of catalyst 3 were heated for 2 hr in H_2 after TPR and then reused in further oxidation–TPR cycles.

Electron Microscopy

Catalyst samples were dispersed ultrasonically in ethanol. A drop of the dispersion was then placed on a holey carbon film supported on a 400-mesh Cu grid, dried, and examined in a JEM 100 CX electron microscope.

X-Ray Diffraction

Stepscans in the $2\theta/\theta$ mode were obtained with a vertical D-500 diffractometer on a K805 generator (Siemens A.G.) using an FK50/21 Cu fine-focusing tube operated at 45 kV and 20 mA with a Ni filter, a slit setting at 0.3°, 0.3°, 0.3°, 0.15°, and rotating specimens. Samples were either loosely back filled into 4-mm thick holders as suggested originally by McCreery and described recently in (*7*), or they were pressed at 8000 kg into tablets and then mounted in the holder. The packing did not noticeably influence peak shapes, so when specimens were to be used for further oxidation or TPR experiments they were loosely packed, but pressed tablets were used to determine exact peak positions.

Particle Size Determination

The metal particle sizes in the catalysts were determined by counting and sizing several thousand images of particles on TEM plates taken at a magnification of 160,000×. Average particle sizes obtained were in agreement with those calculated from H_2 adsorption measurements, but values obtained from the shapes of 111 metal peaks in XRD traces were up to 100% higher. This discrepancy probably resulted mainly from the difficulty in determining accurately what proportion of the intensity in the tails of XRD peaks was due to the metal particles or to the substrate.

RESULTS

CHARACTERIZATION OF CATALYSTS

Fresh Catalysts

Examination of TEM images revealed for all catalysts that the metal particles were generally isolated and well dispersed over the surface of the support (Fig. 1). Particles with diameter (*d*) less than about 5 nm

FIG. 1. Electron micrograph showing Ir metal particles on SiO_2 (catalyst 2). The SiO_2 is supported on a thin carbon film which results in a uniform light

usually exhibited spherical shapes, but particles with $d > 10$ nm tended to be flat islands. Furthermore, contrast changes across individual particles showed that those with $d > 5$ nm were often faulted or consisted of different grains. No changes in contrast could be detected across particles with $d \leq 2$ nm and it was assumed that these were mostly single crystals.

However, marked differences existed between catalysts of different metal composition with regard to the size distribution of particles (Figs. 2 and 3). For Ir catalysts, d was generally less than 10 nm and most of the particles were found in the range $0 < d < 1$ nm. In Pt catalysts and Pt/Ir catalysts containing 50% or more of Pt, in contrast, particles with $d > 10$ nm could readily be observed and the size distributions showed maxima at around 2–3 nm.

Examination of catalysts with X-ray diffraction yielded the following general results:

1. The traces of all catalysts showed distinct but broad metal peaks and a sloping background resulting from the support. The separation and change in intensity of the peaks showed that the structure of metal particles was always fcc. When specimens consisted of equal mixtures of Pt and Ir catalysts, the presence of both metals was clearly indicated (see trace marked Pt + Ir in Fig. 4).

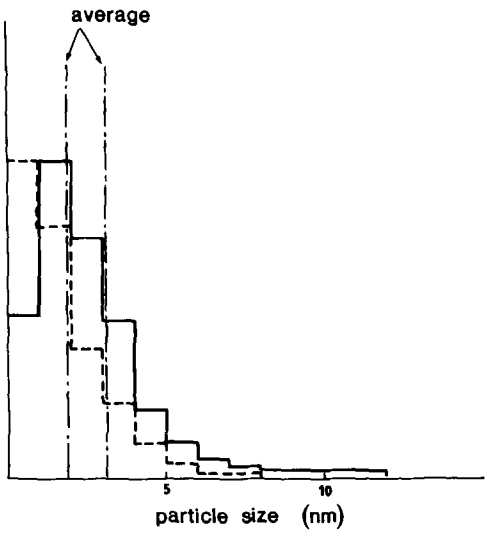

FIG. 2. Histograms showing metal particle size distributions for catalysts 2 (——) and 3 (——) as prepared.

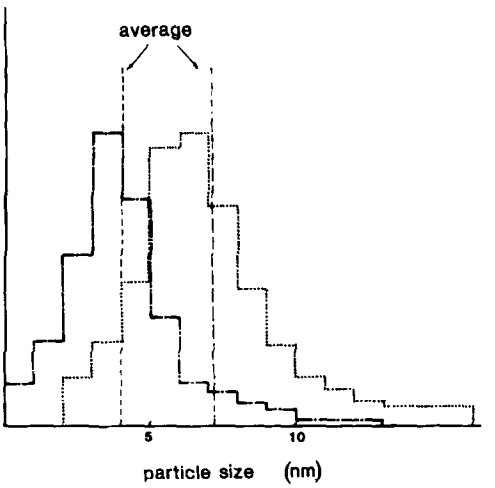

FIG. 3. Histograms showing metal particle size distributions for catalyst 1 after different treatment; as prepared (– · –), heated in O_2 at 700°C for 4 hr. then H_2 at 500°C for 4 hr. (· · · · ·).

2. In the 2θ region between the 111 Pt and Ir peaks, coimpregnated Pt/Ir catalysts exhibited a smooth single peak when the concentrations of the two metals were about equal; but when the concentrations differed markedly two peaks were indicated in this region (compare traces for catalysts 3, 4, and 5 in Fig. 4). Thus XRD showed that mainly single-phase alloy particles were present in coimpregnated catalysts only when the Pt/Ir ratio was close to 50/50.

3. Examination of pressed tablets revealed that 111 peak positions for Pt and Ir occurred at 39.80 and 40.64° 2θ, respectively, as expected from listed d spacings. For Pt/Ir (53/47) the 111 peak position occurred at 40.0° 2θ. With loosely packed specimens (Fig. 4) the peak positions were somewhat displaced towards lower values of 2θ.

In order to avoid complications due to the presence of different phases in the same catalyst the following sections are re-

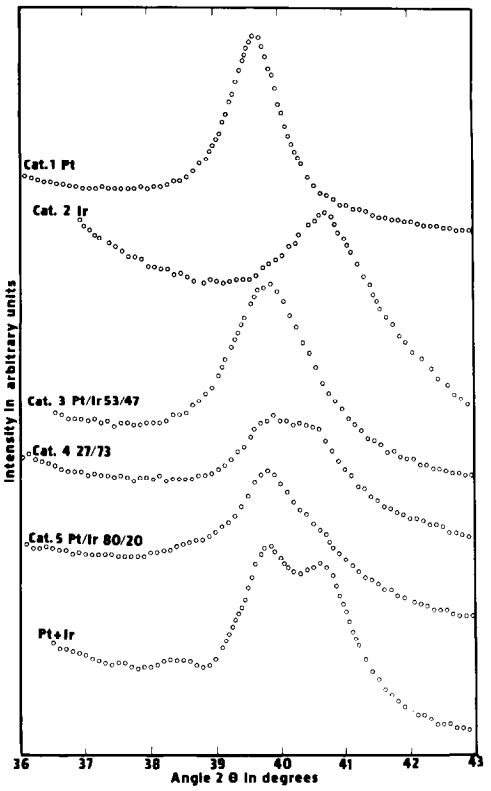

FIG. 4. XRD stepscans across the 2θ region of 111 peaks of Pt (39.80°) and Ir (40.64°) for different catalysts, Cu$K\alpha$ radiation, samples loosely packed. The sloping background results from the SiO_2 catalyst support. The scan labeled Pt + Ir was obtained from an equal mixture of 1.5% Pt on SiO_2 and 1.5% Ir on SiO_2. Each circle represents an individual reading. The intensity units are the same for all samples and the peak height for catalyst 1 amounts to more than 20,000 counts above background.

stricted mainly to catalysts 1, 2, and 3 which contained Pt, Ir and Pt/Ir (53/47) respectively (Table 1).

TABLE 1

Composition of Catalysts

Catalyst number	Total metal content (wt%)	Proportion of constituents (mol%)	
		Pt	Ir
1	0.9	100	0
2	1.7	0	100
3	2.6	53	47
4	2.84	80	20
5	2.2	27	73

CATALYTIC MEASUREMENTS

The extent of conversion and product distribution for n-heptane over catalysts 1, 2, and 3 are summarized in Table 2.

Catalysts Exposed to Oxygen

$100 \leq T_{ox} \leq 300$°C. In this range no changes were observed with XRD, TEM, or SAED for any one of the catalysts.

$300 < T_{ox} \leq 700$°C. For Pt (catalyst 1), the metal peaks in XRD traces developed sharper maxima while in TEM images metal particles developed crystallographic shapes and the average size increased (Fig. 3) as T_{ox} was raised.

For Ir (catalyst 2) and Pt/Ir (catalyst 3), in contrast, marked changes were observed in this range. The changes depended on T_{ox} but not on the choice of system given in the experimental section.

As illustrated with XRD traces over the range $26 \leq 2\theta \leq 36°$ in Figs. 5 and 6, with

TABLE 2

n-Heptane Conversion at 400°C

Catalyst	Conversion (%)	Product Distribution (%)[a]			
		$<C_7$	*iso*-C_7	*cycl*-C_7	toluene
(1) Pt	10	14	40	20	26
(2) Ir	100	100 (Methane)	—	—	—
(3) Pt/Ir	53	19	34.5	22.5	24

[a] Expressed as percentages of *n*-heptane converted to indicated products.

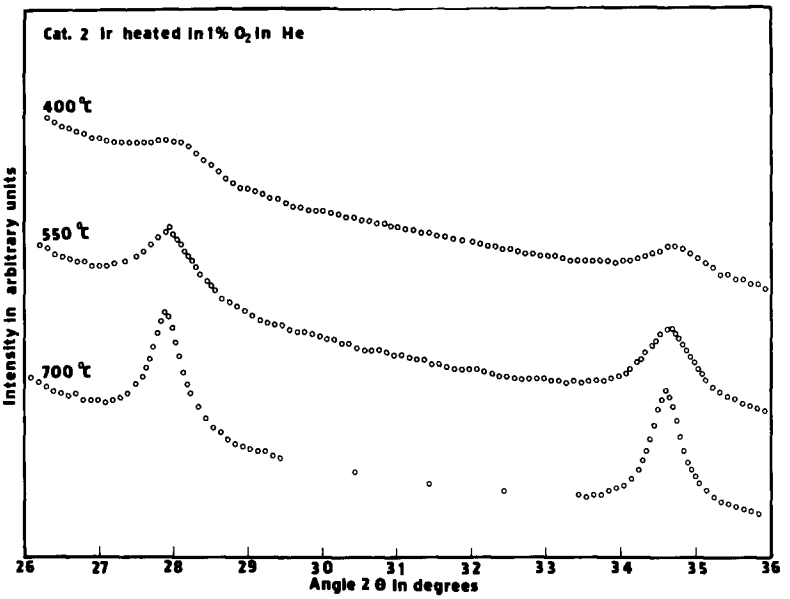

FIG. 5. XRD stepscans across the 2θ region of the 110 (28.1°) and 101 (34.75°) peaks of IrO_2 obtained on catalyst 2 treated at the indicated conditions, Cu$K\alpha$ radiation. The sloping background results from the SiO_2 catalyst support. The intensity units are the same for all scans.

both catalysts new peaks occurred at identical 2θ values. These peaks became first detectable at $T_{ox} \approx 400$°C and developed definite maxima as T_{ox} was increased to 700°C. When the catalyst contained only Ir (catalyst 2) all the additional peaks could be systematically identified as resulting from the formation of tetragonal IrO_2 with rutile structure (*8*, *9*).

As T_{ox} increased, the metal peaks changed in different fashions for catalysts 2 and 3. For Ir (catalyst 2) the peaks decreased in height and they became markedly broader until at $T_{ox} = 550$°C they were no longer detectable. (A low broad peak, which was observed at $2\theta = 40.1°$ resulted from {200} type planes of IrO_2.) Thus, for this catalyst, oxidation of Ir was complete after 1 hr at $T_{ox} = 550$°C.

With Pt/Ir (catalyst 3), in contrast, the metal peaks became appreciably sharper and the maxima shifted toward the positions of the appropriate bulk reflections of Pt. This indicated that the remaining metal particles increased generally in size and that they became enriched in Pt. Thus, as with pure Pt (catalyst 1), in Pt/Ir (catalyst 3) the Pt was also not oxidized to any appreciable extent and the oxide was in this case also essentially IrO_2. This result could not be deduced from the appearance of the oxide peaks alone because PtO_2 and IrO_2 have very similar structures and agree closely in their interplanar spacings (*9*).

Examination of TEM images (Figs. 7, 8) showed for both Ir and Pt/Ir that the oxides generally grew as individual crystals forming thin blades or sheets which decreased in thickness towards the edges. Only with Ir (catalyst 2) heated at $T_{ox} = 550$°C in air under static conditions were metal particles occasionally enveloped by fine-grained polycrystalline oxide (Fig. 7b).

In the range $400 < T_{ox} < 550$°C the oxide crystals were often still attached to what appeared to be the original metal particles. This is illustrated in Fig. 7c, which also shows that in this range of T_{ox}, small particles exhibiting different contrast were usually distributed all over the oxide when the catalyst contained Pt/Ir. No such particles

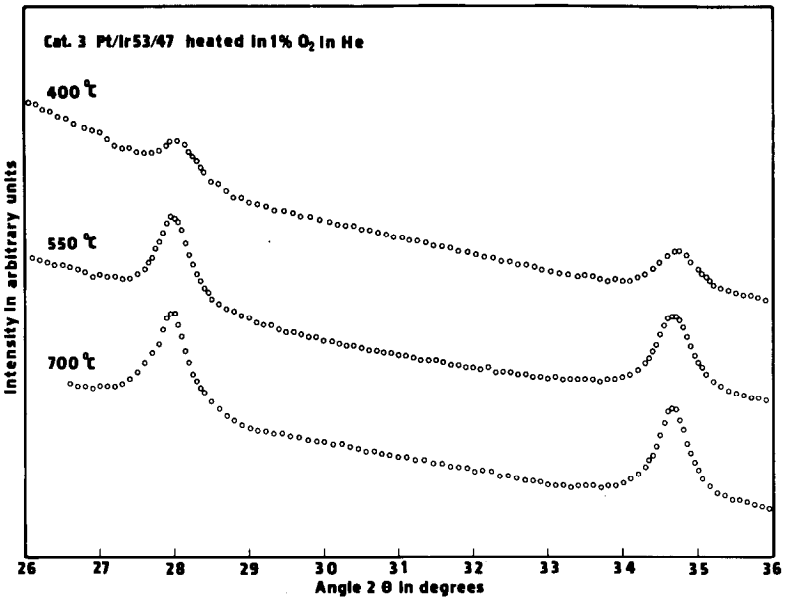

FIG. 6. XRD stepscans across the 2θ region of the 110 (28.1°) and 101 (34.75°) peaks of IrO_2 obtained on catalyst 3 treated at the indicated conditions, Cu$K\alpha$ radiation. The sloping background results from the SiO_2 catalyst support. The intensity units are the same for all scans.

were observed with Ir (catalyst 2). Observations in dark-field illumination showed that the particles which were distributed all over the oxide were metal, but it was not possible from the SAED patterns to distinguish between Pt and Ir.

In the range $550 < T_{ox} \leq 700$°C (Figs. 7d, 8a–d) oxide attached to original metal particles was no longer observed with Ir catalysts but was still common with Pt/Ir up to $T_{ox} = 600$°C (Fig. 7d) and was occasionally observed even at $T_{ox} = 700$°C (Fig. 8c). However, as shown in the figures, metal particles were no longer distributed all over the oxide if T_{ox} exceeded about 550°C. The average size of oxide particles was much larger at the higher values of T_{ox} and both blades and sheets were somewhat thicker; in addition, the larger residual metal particles in Pt/Ir catalysts exhibited crystallographic shapes, while the smaller ones formed nearly perfect spheres, (e.g. see Figs. 8d and 12b). Twinning was present frequently in the oxide and caused many of the blades to adopt sharply bent shapes like boomerangs, but sometimes growth had also proceeded normal to the plane of a boomerang (Fig. 8a). Often one of the twins was terminated by crystallographic planes while the other exhibited cavities (Fig. 8b). Occasionally both ends were crystallographic and there were signs that the twins had been attached to a substrate at their junction. The longest twin arms observed for $T_{ox} \approx 700$°C were somewhat longer than 1 μm. Even such long blades were very thin, had parallel sides, were terminated by crystallographic planes and had length to width ratios of up to 100 to 4. Examination of lattice images and SAED patterns of oxide (Fig. 9) revealed that the planes of blades and elongated sheets were always of the {110} type and that the growth direction was always parallel to the c axis (Fig. 9a). The crystallographic terminations of the blades were thus formed by {111} and {002} type planes. Thin sheets which were not elongated were usually smaller in size. Lattice images of such oxide sheets (Fig. 9b) showed that in this case the plane of the sheet was parallel to {002} type planes.

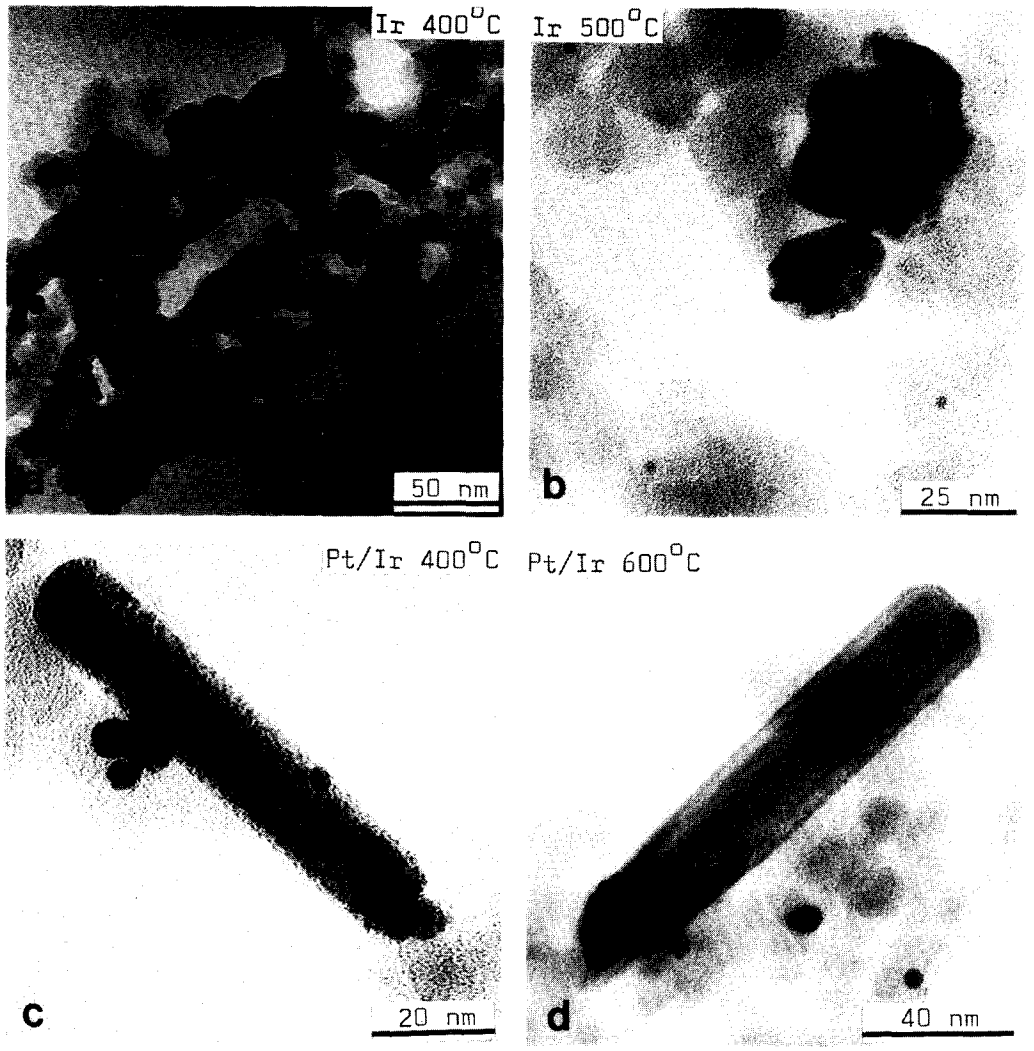

FIG. 7. Electron micrographs illustrating the oxidation of catalysts up to 600°C. The oxide, IrO_2, forms thin blades or sheets attached to metal particles in flowing 1% O_2 in He, [(a), (c), and (d)] but in static air it occasionally encapsulates metal particles (b). Below 550°C small Pt particles are distributed over the oxide in Pt/Ir catalysts (c).

TRP PROFILES

For Pt (catalyst 1) exposed to oxygen in the range $100 < T_{ox} < 700$°C, the TPR profiles exhibited only a small negative peak with a minimum at 130°C which was attributed to the desorption of adsorbed hydrogen. The absence of positive peaks with TPR agrees with the failure to detect oxide with either XRD or TEM. The reduction of chemisorbed oxygen on Pt occurs already below 25°C (*28*), and therefore does not contribute to the TPR profiles.

For Ir (catalyst 2), selected profiles which illustrate the behavior of this catalyst are shown in Fig. 10. When T_{ox} was increased above ambient, a single TPR peak with a maximum at 75°C appeared as T_{ox} reached 100°C. When T_{ox} was increased further (150, 200, 250°C) the peak became higher and the maximum shifted to 87°C. At $T_{ox} \approx 300$°C a second peak with maximum

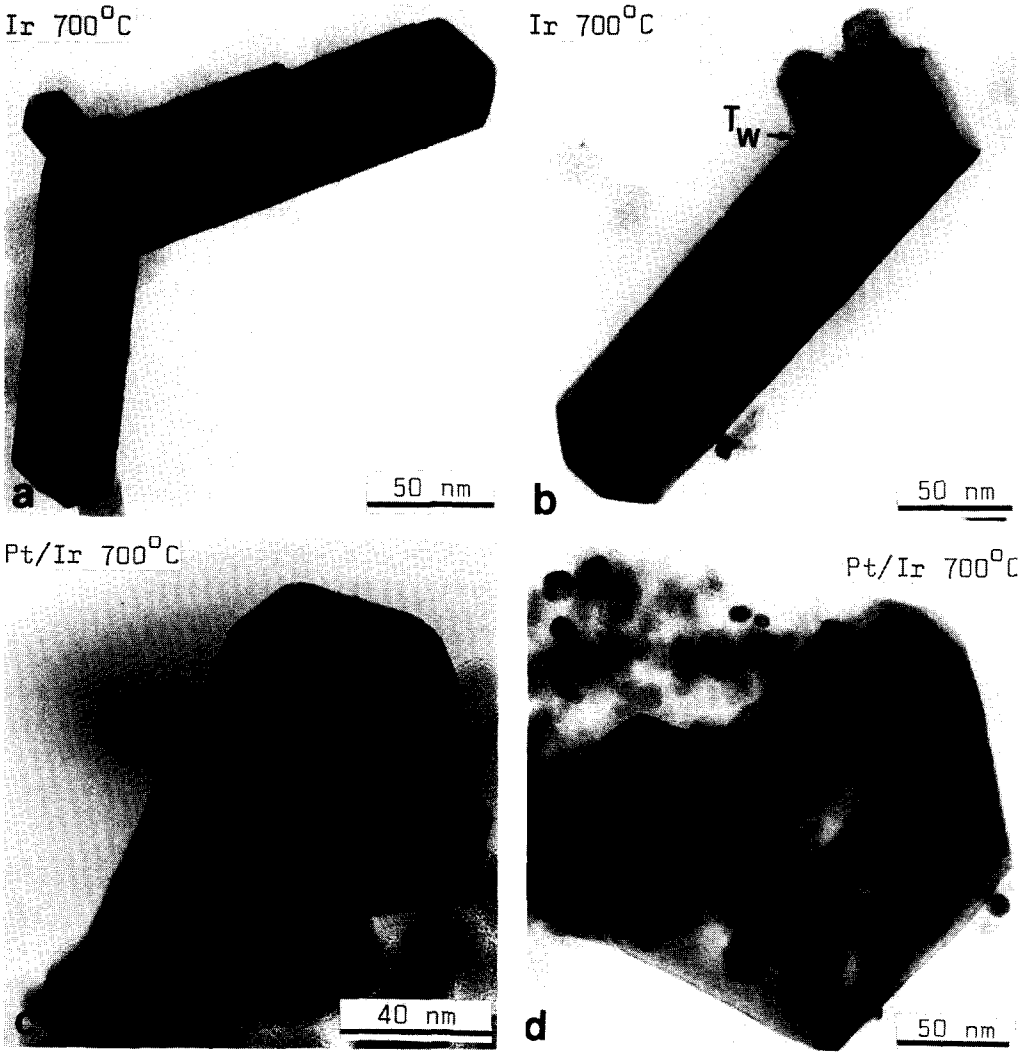

FIG. 8. Electron micrographs showing typical oxide, IrO_2, crystals formed in flowing 1% O_2 in He in the range 600–700°C. Metal particles are still present in Pt/Ir catalyst mostly separated from the oxide (d), but sometimes still attached to it (c). Twinning is common in the oxide, e.g., see $T_w \rightarrow$ (b).

at 215°C became discernible. This peak increased rapidly as T_{ox} was raised further while the peak at 87°C decreased until at $T_{ox} \approx 550$°C only the high-temperature peak remained and its maximum was now at 240°C. Increasing T_{ox} above 550°C did not produce any further changes in the TPR profile.

For Pt/Ir (catalyst 3) (Fig. 11) again a single TPR peak appeared as T_{ox} reached 100°C, but the maximum of the peak was at 60°C. As T_{ox} was increased to 300°C the peak height increased but the temperature of the maximum remained constant. At $T_{ox} = 300$°C again a second peak appeared with a maximum at 215°C. The general behavior of the two peaks with increasing T_{ox} was similar to that observed with Ir (catalyst 2). For example, the low-temperature peak decreased and was no longer detectable at $T_{ox} = 550$°C. However, in contrast to Ir, the maximum of the high-temperature peak remained constant at 215°C but the peak developed a shoulder on its high-tempera-

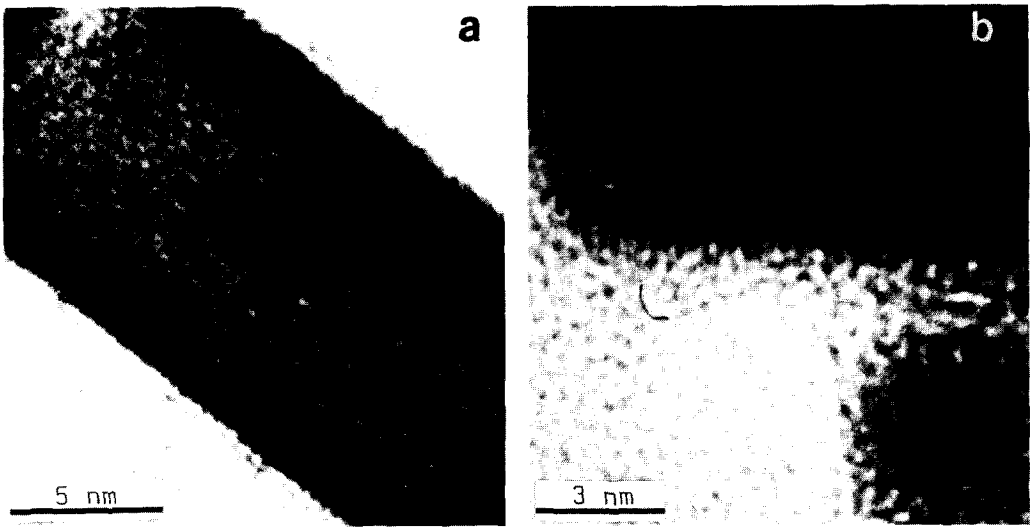

FIG. 9. Electron micrographs showing lattice images of 110-type planes in oxide, IrO_2; blades (a) and sheets (b).

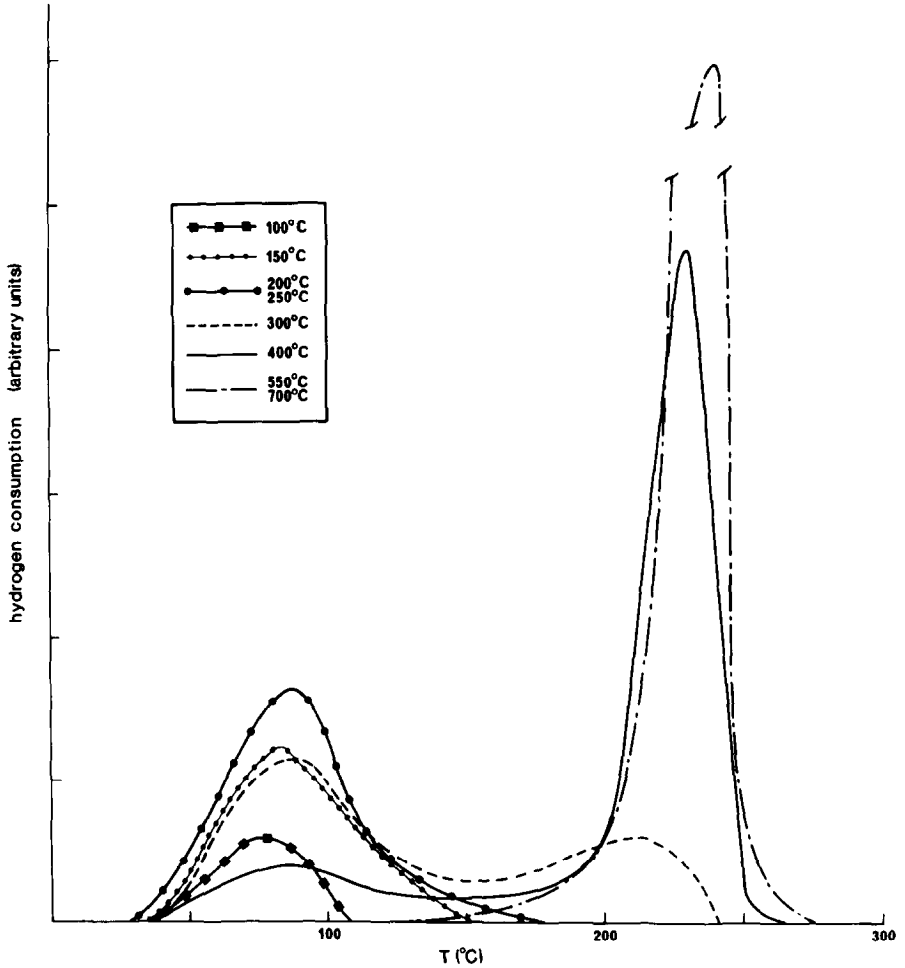

FIG. 10. Temperature-programmed reduction (TPR) profiles typical for Ir (catalyst 2) oxidized at indicated temperatures.

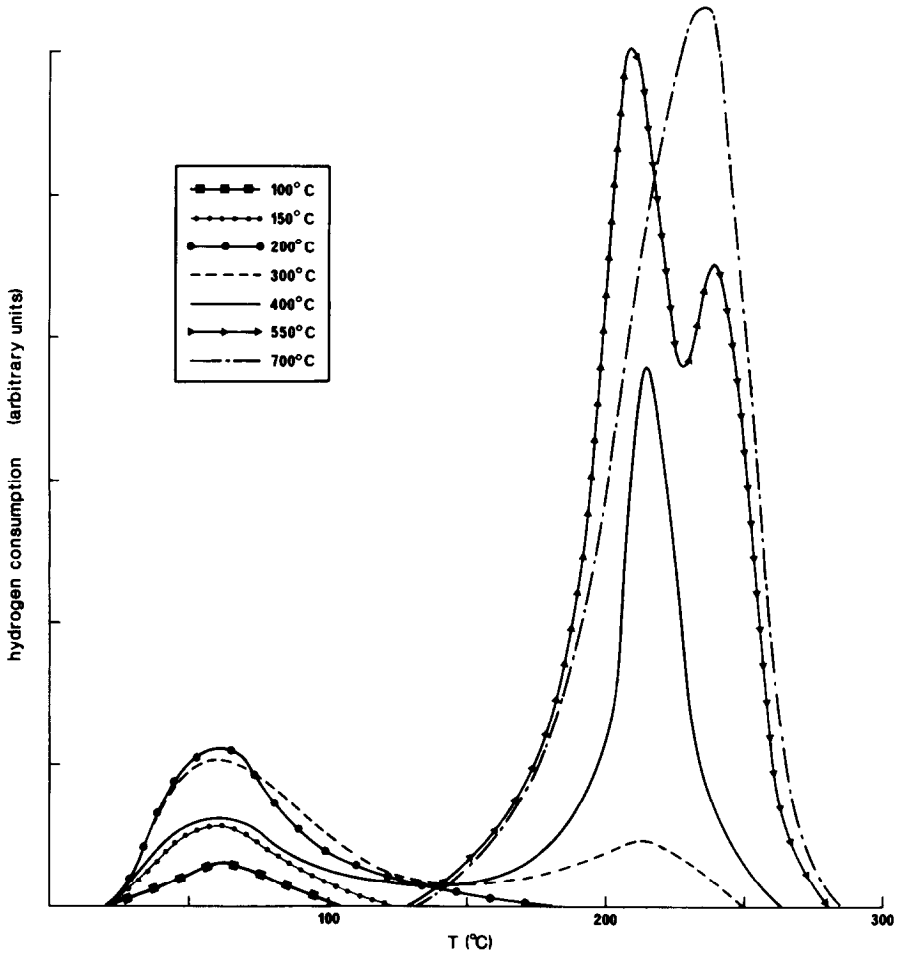

FIG. 11. Temperature-programmed reduction (TPR) profiles typical for Pt/Ir (catalyst 3) oxidized at indicated temperatures.

ture slope and as T_{ox} reached 550°C a marked satellite maximum at 240°C was obvious. Raising T_{ox} above 550°C increased the height of the maximum at 240°C and decreased that of the maximum at 215°C so that at T_{ox} = 700°C the profile exhibited mainly a single peak which had a maximum at 240°C and a barely discernible shoulder at 215°C.

Quantative data extracted from the TPR profiles are summarized in Table 3 together with the mean particle sizes and the number of surface atoms for catalysts 1, 2, and 3. When the H_2 consumption during reduction was calculated from the areas under the TPR peaks it was found that for Ir (catalyst 2) the consumption levelled off in the region $200 < T_{ox} < 300$°C and when T_{ox} was larger than 550°C, whereas for Pt/Ir (catalyst 3) it increased monotonously with T_{ox} (Table 3, Fig. 14).

When a sample of Pt/Ir (catalyst 3) which had been subjected to an oxidation (200°C)–TPR cycle was heated in H_2 at 400°C for 2 hr and then reoxidized at T_{ox} = 200°C the new TPR profile showed a marked increase in the area under the peak. However, the original profile was restored when the catalyst sample was heated in H_2 at 400°C for 20 hr after the second TPR profile (Table IV).

To study the reduction mechanism, TPR profiles for T_{ox} = 550°C were interrupted at

TABLE 3

Quantitative TPR Data

Catalyst	No. of surface metal atoms ($g_{cat}^{-1} \times 10^{19}$)[a]	Mean Particle Size (nm)	Temp. of oxidation, T_{ox} (°C)	Maxima of TPR peaks (°C)		H_2 consumed in oxide reduction (10^{19} molecules g_{cat}^{-1})		
				Low-temp. peak	High-temp. peak	Low-temp. peak	High-temp. peak	Total
Catalyst 1			100					
Pt/SiO_2	0.75	4.0	700	no peaks		—	—	—
Catalyst 2	3.1	1.9	100	75		1.45	—	1.45
Ir/SiO_2			150	85		3.61	—	3.61
			200	87		4.52	—	4.52
			250	87		4.58	—	4.58
			300	87	215	3.43	1.81	5.24
			400	87	230	1.39	6.08	7.47
			550		240	—	10.60	10.60
			700		240	—	11.00	11.00
Catalyst 3	3.0	3.1	100	60		0.36	—	0.36
$Pt/Ir\ (53/47)/SiO_2$			150	60		0.78	—	0.78
			200	60		1.20	—	1.20
			250	60		1.63	—	1.63
			300	60	215	1.69	1.01	2.70
			400	60	215	0.84	2.59	3.43
			550		210 240	—	4.40	4.40
			700		240	—	5.00	5.00

[a] From H_2 adsorption.

240°C for Ir (catalyst 2) and at 215°C for Pt/Ir (catalyst 3) (Figs. 10, 11). When the profiles were restarted after the catalysts had been cooled to room temperature in N_2, both catalysts then displayed profiles with just a single maximum at 215°C similar to the high-temperature prts of uninterrupted profiles for T_{ox} = 400°C. Examination of TEM images revealed that when the TPR runs were interrupted, oxide crystals in both catalysts carried some firmly adherent metal crystals which had been nucleated in the TPR run (compare Figs. 12a–c, 8). The concentrations of metal particles increased towards the edges of an oxide crystal (Fig. 12b).

Moiré fringes (Fig. 12a) indicated that the metal was not preferentially oriented with respect to the oxide. When the oxide was thin, gaps could be seen between the metal particles and the oxide (Fig. 12c). Examination with XRD revealed slightly reduced IrO_2 peaks. For Ir (Catalyst 2) the peak at around 40° 2θ was slightly increased and for Pt/Ir a shoulder was noticeable on the 111 metal (Pt) peak, similar to that resulting from reduction after oxidation at T_{ox} = 400°C (Fig. 13). These observations indicated that the partial reduction of the oxide produced separate Ir particles.

After a TPR profile was completed, XRD traces no longer revealed any oxide peaks. For pure Ir (catalyst 2) the 111 metal peak was more prominent and sharper than before oxidation, while for Pt/Ir two distinct

TABLE 4

Repeated Oxidation (T_{ox} = 200°C)–TPR Experiments on Catalyst 3 (Pt/Ir(53/47))

Catalyst treatment		TPR peak area (10^{19} molecules $H_2\ g_{cat}^{-1}$)	Surface composition (mol% Ir/Pt)
Fresh catalyst			
$1\%O_2/He$	200°C 1 hr	1.23	27/73
H_2	400°C 2 hr		
$1\%O_2/He$	200°C 1 hr	2.05	46/54
	400°C 20 hr		
	200°C 1 hr	1.30	29/71
	400°C 2 hr		
	200°C 1 hr	2.17	48/52
	400°C 20 hr		
	200°C 1 hr	1.27	28/72

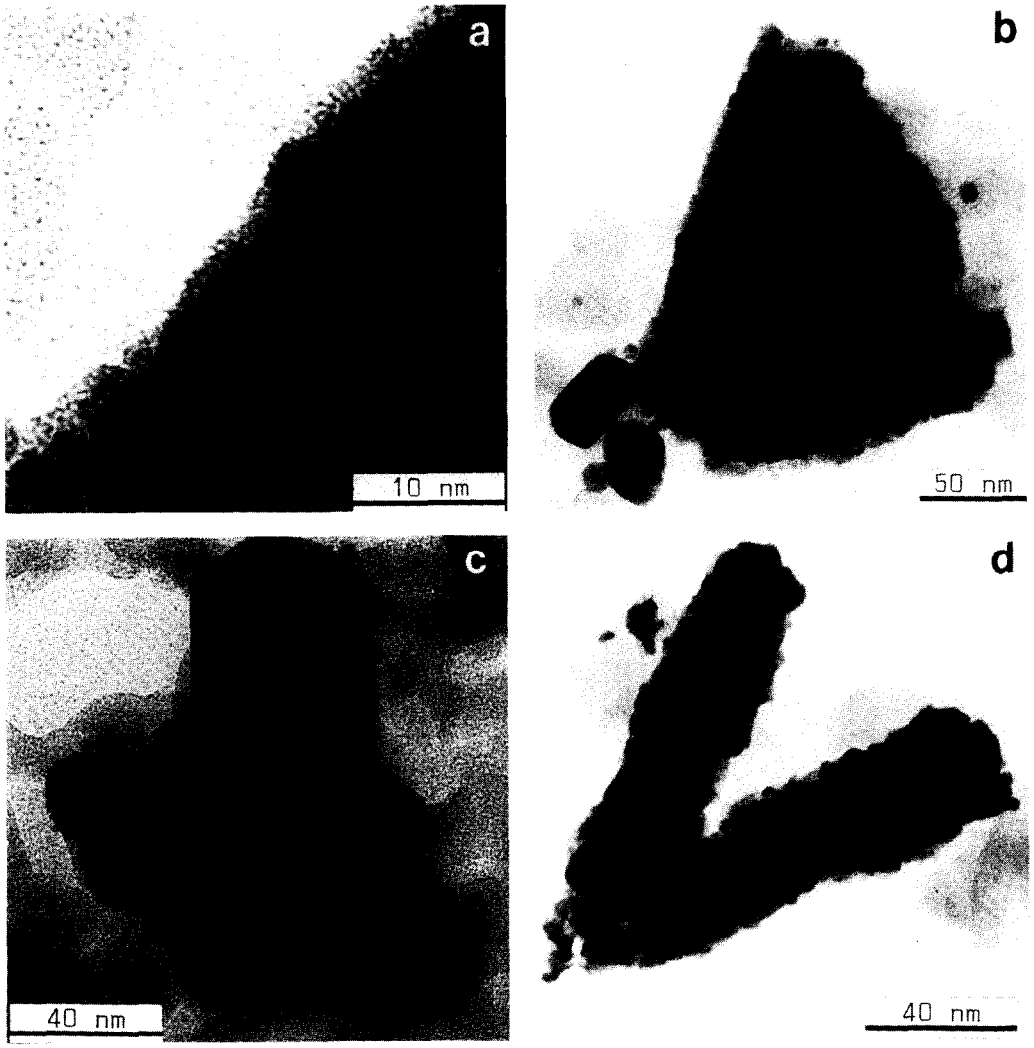

FIG. 12. Electron micrographs illustrating the partial [(a), (b), (c)] and complete reduction (d) of IrO_2 crystals. The temperature-programmed reduction was terminated at 215°C for Pt/Ir [(a), (b)] and at 240°C for Ir (c). In (a), which shows part of (b) at higher resolution, moiré fringes show that the metal and oxide are not specifically aligned. Large residual metal, Pt-rich, particles are obvious in (b). Complete reduction leads to aggregates of small heavily faulted Ir particles preserving the general shape of the oxide crystal (d).

111 metal peaks were observed (Fig. 13) showing that such treatment destroyed the alloy (cf. Figs. 4 and 13). TEM images revealed that the more substantial oxide crystals had been converted into contiguous aggregates of extensively faulted and defect Ir crystals. These aggregates often preserved the shape of the original oxide particles (Fig. 12d). Generally thinner oxide crystals and sheets produced smaller and less defective metal particles and more tenuous aggregates.

DISCUSSION

Catalyst Structure

As shown in the results, we deduce from the XRD traces that exclusively single-phase Pt/Ir alloy particles were formed only when the two metals were present in very similar concentrations. This result dis-

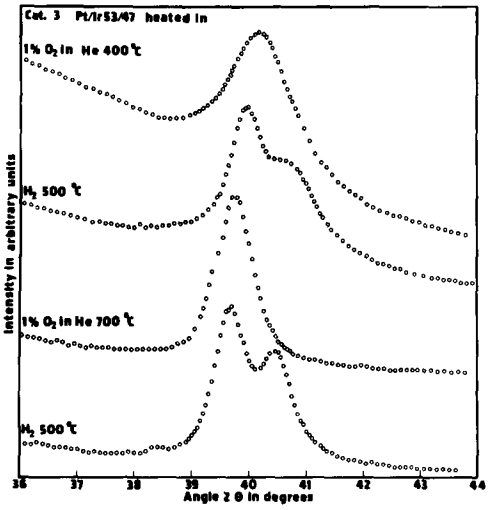

FIG. 13. XRD stepscans across the 2θ region of the 111 peaks of Pt (39.80°) and of Ir (40.64°) for Pt/Ir (catalyst 3) oxidized and subsequently reduced at the indicated conditions. The intensity units are the same for all samples.

agrees with findings by Rasser *et al.* (*10*) that the two metals form single-phase alloys in all proportions if prepared as Kulifay powders or by coimpregnation onto γ-Al_2O_3 and subsequent calcination in air at 550°C and reduction at 380°C. However, when we tried to prepare Pt/Ir alloy catalysts on γ-Al_2O_3 by coimpregnation (*2b*) we found that calcination in air above 300°C resulted in separate Pt and Ir particles in agreement with Garten and Sinfelt (*2b*).

The lattice constant (0.390 nm) deduced from the XRD peak positions observed with Pt/Ir (catalyst 3) tablets corresponds to a solid solution composition of only 20 at.% Ir (*11*). A similar observation has been reported for Pt/Ir (50/50) on SiO_2 by Sinfelt and Via (*2a*). In that work the total metal concentrations in the catalysts were 20, 10, and 5% and it was found that while for the higher concentrations the XRD peak positions indicated a solid solution concentration of 50 at.% in Ir, for the 5% metal concentration catalyst, the peak positions indicated a solid solution concentration of only 32 at.% in Ir. As an explanation, the authors assumed the presence of Ir-rich particles which were characterized by a metal dispersion higher than that of the catalyst overall, so that these particles would not influence the XRD peak position. However, they did not determine particle size distributions directly. In the present work TEM showed that very small particles were present in Pt/Ir (catalyst 3) only in small concentrations (Fig. 2) and its catalytic behavior was like that of Pt rather than Ir (see Table 2). Catalysis is a sensitive test for the presence of separate Ir particles, since for the reaction of *n*-heptane, Ir is about 10^4 times more active than Pt and leads mainly to hydrogenolysis (*12*). Thus from all evidence, small Ir particles were not present in catalyst 3 and the explanation suggested by Sinfelt and Via (*2a*) is not applicable.

There is one effect which may lead to a virtual bimodal particle size distribution. This is the surface enrichment of particles with Pt, which is expected at equilibrium from a consideration of the surface energies of the two metals (*13*). Surface enrichment in Pt has been observed on Pt/Ir alloy films by Kuijers and Ponec with Auger analysis (*14*), and is indicated for the present catalysts from the TPR profiles (*vide infra*), and from ESCA measurements (*15*). Such a bimodal distribution of particles would not be obvious if the images of metal particles are measured in bright-field illumination, but it might show up when the diffracted beams are used as, for example, here with X rays. However, the indicated segregation does not lead to a distribution which is wide enough so that one could expect the Ir-rich interiors not to influence the peak position. In a study on the phase separation of Pt/Ir solid solutions of bulk specimens Raub and Plate (*16*) have reported that while sharp XRD reflections were readily observed for Pt-rich phases, Ir-rich phases were indicated only by extremely weak and diffuse signals or could not be detected at all even after prolonged annealing at high temperature (up to 1 year at 700°C). These authors attributed their results to very slow diffu-

sion of Ir which prevented the Ir-rich phases from forming ordered structures. However, our XRD results reveal well-defined peaks after heating at much lower temperatures even for pure Ir (catalyst 2). Thus the explanation of those authors is also not applicable and the observations made here and previously (*2a*) appear to reveal an as yet inexplicable phenomenon.

Exposure to Oxygen

$300 < T_{ox} \leq 700°C$. The conclusion from the XRD and TEM results that only Ir is oxidized to any appreciable extent when catalysts are heated in oxygen in this range is confirmed by the TPR profiles (Figs. 10, 11) which show that positive peaks occur only with Ir (catalyst 2) and Pt/Ir (catalyst 3) but not with Pt (catalyst 1). The high reduction temperature (maxima >200°C) which is similar to that observed for the reduction of H_2IrCl_6 (*17*) is also in agreement with the conclusion that the oxide is IrO_2.

When T_{ox} exceeded 500°C an appreciable increase in average size was observed for: (i) the residual, Pt-rich, particles in catalyst 3 (cf. XRD traces in Figs. 4 and 13); (ii) the Pt particles in catalyst 1 (cf. histograms in Fig. 3; and (iii) the IrO_2 crystals in catalysts 2 and 3 (cf. Figs. 5–8). The increase in metal particle size (catalysts 1 and 2) is probably due to the formation and decomposition of volatile oxide of Pt (*18*), the presence of which we failed to detect. From TEM work on Pt vapor deposited onto a thin film of SiO_2, it has been suggested that Pt oxide may be transported in molecular form through the gas phase or across the substrate (*19*). In the present work, with the large area of support, only transport through the gas phase is likely to be important. The same process most likely applies also to the disappearance, at $T_{ox} \geq 550°C$, of the finely divided metal which was distributed at lower T_{ox} all over IrO_2 crystals still attached to original Pt/Ir particles (cf. Figs. 7c and d). Because this type of distribution of metal never occurred with pure Ir (catalyst 2), we believe we observed here small islands of Pt.

The increase in IrO_2 crystal size became noticeable only at a value of T_{ox} where in the Ir catalyst all the metal had already been oxidized: At the highest values of T_{ox} many IrO_2 crystals were several orders of magnitude larger than even the biggest original metal particles observed in the catalysts. We therefore conclude that this growth resulted from transport of oxide through the gas phase. Such transport has been attributed to the formation of IrO_3 (*20*). In the present work an increase in average crystal size of IrO_2 similar to that in oxygen was observed when an Ir catalyst fully oxidized at $T_{ox} = 550°C$ was heated in N_2 in the range 550–700°C. In this case, gas phase transport of IrO_2 must have occurred, in agreement with other reported results (*21*).

That very regularly shaped single or twinned crystals should result from gas phase transport may seem surprising. However, similarly shaped large single or twinned crystals have also been reported for other oxides with rutile structure grown under conditions where material transport through another phase took place, for example, with TiO_2 grown from borate fluxes (*22*). In the present work, oxidation at $T_{ox} \leq 550°C$ showed that the shapes of IrO_2 crystals are generated under conditions where transport through the gas phase is still negligible. We believe that, while still attached to original metal particle, oxide crystals "grow" at their interface with the metal and the shapes reflect epitaxial metal–oxide relationships. If, at this stage, oxide crystals "grew" at their perimeter, Ir oxide in molecular form would have to diffuse from the original metal particles onto the attached IrO_2 crystals. If such a process were operating we would expect most oxide blades to be tapered toward the tip. The results, in contrast, show that blades were often tapered toward the point of attachment to the original particle (Fig. 7d), indicating

that the interface shrank as the metal was used up in the oxidation. In the present work, growth sustained by material transport through another phase thus does not initiate the crystal shapes originally. However, in contrast to other situations (*22*), it is surprising how well the shapes are preserved, since examination of lattice images shows that even blades several thousands of angstroms long were found to be parallel side on an atomic scale.

For Ir (catalyst 2) the oxidation of metal particles is complete at $T_{ox} \geq 550$°C as evidenced by the absence of metal particles in TEM images, the disappearance of Ir metal reflections in XRD traces, and the saturation of the H_2 consumption during TPR (Fig. 14, Table 3). Now, a comparison of the H_2 consumption at $T_{ox} > 550$°C with the Ir content of the catalyst as prepared (Table 1) yields a ratio of molecules of H_2 to IrO_2 of slightly greater than 2 and thus establishes the following reduction equation:

$$IrO_2 + 2H_2 \rightarrow Ir + 2H_2O.$$

The H_2/IrO_2 ratio is greater than 2 because H_2 is adsorbed on the reduced metal. This process contributes very little to the H_2 consumption because the oxidation → TPR treatment reduced the number of Ir surface atoms to about 14% of the initial value (see Table 2) and at the temperature

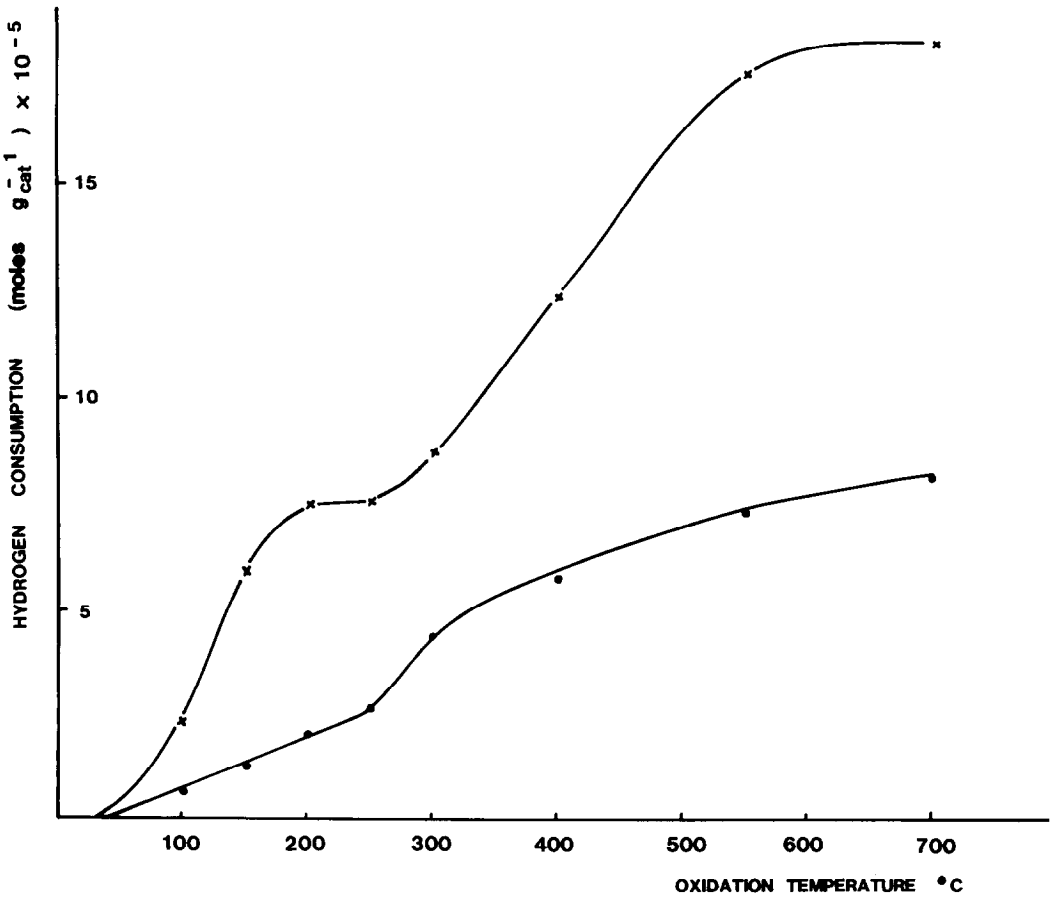

FIG. 14. Hydrogen consumption, calculated from the temperature-programmed reduction, TPR, peak area, plotted as a function of the oxidation temperature, T_{ox}, for Ir (catalyst 2) (×), and Pt/Ir (catalyst 3) (●).

of reduction of IrO_2 (>200°C) the H_2 coverage is only about 30% of the value obtained at 25°C (*23*). Using the above stoichiometry, one obtains from the H_2 consumption for Pt/Ir (catalyst 3) that only 65% of the Ir originally present in the catalyst (Table 1) has been oxidized at T_{ox} = 700°C. This result is not surprising, because oxidation of Ir is expected to become quickly limited by diffusion of Ir atoms to the alloy surface.

100 < T_{ox} ≤ 300°C. In this range no oxide could be detected with XRD and TEM but again in the TPR profiles positive peaks were observed for Ir (catalyst 2) and Pt/Ir (catalyst 3) (Figs. 10, 11) but not for Pt (catalyst 1). We therefore conclude that we are dealing here also with an oxide of Ir only. Because the low temperature of reduction (maxima < 100°C) implies an oxidation state of Ir of less than 4+, the oxide is probably a surface oxide (Ir_sO) similar to that reported by Brooks (*24*). Indeed, if we compare the H_2 consumption during TPR for Ir (catalyst 2) heated in the range 200 ≤ T_{ox} ≤ 300°C with the number of surface Ir atoms before oxidation (Fig. 14, Table 3) we obtain the same stoichiometric relationship as Brooks, namely,

$$Ir_sO + 1.5H_2 \rightarrow Ir_sH + H_2O.$$

We believe that the saturation values of the H_2 consumption during TPR as determined here provide a better measure of metal surface areas of Ir catalysts than is obtained with O_2–H_2 titrations carried out at higher temperatures. This is illustrated by a consideration of the values reported by Brooks who found that surface areas determined from the reduction of surface oxides were larger than those calculated from hydrogen adsorption (*24*). The present results indicate that his arbitrary selected conditions (15 kPa O_2, 350°C, 30 min) are likely to lead to the formation of some bulk oxide.

With Pt/Ir (catalyst 3), in contrast, the H_2 consumption (Fig. 14) and the height of the low-temperature TPR peak (Fig. 11) increased steadily in the range 100 < T_{ox} < 300°C. This behavior can only be explained if reaction of O_2 with Ir to form Ir_sO causes further Ir to diffuse to the surface. Such oxygen-induced surface segregation of the more readily oxidized component of an alloy is predicted by recent theories (*13*) and has been observed, for example, with Pd/Au (*25*). If the H_2 consumption for Pt/Ir at T_{ox} = 200°C (Fig. 14) is compared with the number of metal surface atoms before oxidation (Table 3) the above stoichiometry gives a surface composition at this temperature of 27% Ir and 73% Pt. However, that value is certainly somewhat too low since during oxidation at 200°C, some Ir will have diffused to the surface.

The extent to which the average surface composition may be changed is illustrated in Table 4.

When a second oxidation–TPR sequence was carried out immediately after the first oxidation–TPR cycle or after only short annealing in H_2 at 400°C, a surface composition of 50% Pt and 50% Ir was calculated from the H_2 consumption. However, prolonged annealing restored the original surface composition of 73% Pt and 27% Ir.

Wagstaff and Prins (*17*) determined TPR profiles for Pt/Ir (50/50) on γ-Al_2O_3 oxidized at 350°C. They observed a single peak with a maximum at 105°C and ascribed this to the reduction of a mixed oxide of Pt and Ir with an overall oxidation state of 3+. This interpretation is not supported by the present results. We have recently discussed the reason for this discrepancy elsewhere (*26*).

Reduction of Oxide

It was observed that interrupting a TPR profile for T = 550°C at the high-temperature maximum and restarting it again at room temperature leads, for both Ir (Catalyst 2) and Pt/Ir (catalyst 3), to a lowering in the temperature of the maximum. This shows that after the interruption the rate of reduction is greater. This speeding up of the reduction is no doubt due to the presence of the metal particles formed before the interruption. However, when Ir metal particles

were physically added to IrO_2 crystals by thoroughly mixing samples of reduced and completely oxidized Ir catalysts, the TPR profile was very much like that observed for the oxidized catalyst alone. These results show that intimate oxide–metal contact reduces the maximum from 240 to 215°C. The same effect is reflected in the TPR profiles for the range $300 < T_{ox} < 700$°C for which the TEM results show that intimate oxide–metal contact exists at the lower end but is lost as T_{ox} increases. Since with Ir all metal is converted to oxide the maximum is shifted to 240°C already at $T_{ox} = 550$°C (Fig. 10), but with Pt/Ir an appreciable proportion of oxide crystals is then still in contact with the residual Pt-rich metal particles and thus both maxima are observed (Fig. 11). Similarly at $T_{ox} = 100$°C, where the surface of Ir metal particles is only partly covered with Ir_sO (Fig. 10) the TPR maximum occurs at 75°C and in the range $200 < T_{ox} < 300$°C, where the surface is completely converted to Ir_sO the maximum is shifted to 87°C. With Pt/Ir, in contrast, where Pt is exposed at all values of T_{ox} the low-temperature TPR maximum is constant at 60°C. Our results thus show that the reduction is autocatalytic. Hydrogen chemisorbs dissociatively on nucleated metal crystals and diffuses in atomic form onto the oxide where it facilitates the nucleation of further metal crystals. Thus a spillover effect similar to that observed for noble metals on NiO is operating (*27*). The generally higher concentrations of metal particles near the thinner edges of oxide crystals (Fig. 12b) suggest that surface steps (terminating {110} type oxide planes) are most active for nucleation.

The result, that on complete reduction IrO_2 crystals are converted into agglomerates of small metal particles (e.g., Fig. 12d), disagrees with claims by Sinfelt and Via (*2a*) who concluded from XRD observations that oxide and metal particles are of similar size. Since Sinfelt and Via prepared catalysts with metal loadings more than 5 times higher than the ones employed here it may well be that the resulting oxide crystals were generally thicker than in the present work. The discrepancy may then be explained since we observed that reduction of thicker oxide crystals produces somewhat larger metal particles.

CONCLUSIONS

1. When H_2PtCl_6 and H_2IrCl_6 coimpregnated on SiO_2 are reduced in H_2 at 500°C, single-phase Pt/Ir alloy particles are formed only if the concentrations of Pt and Ir are nearly equal.

2. Only Ir is oxidized when Pt/Ir alloy particles are heated in an atmosphere of 1% or more of O_2 in an inert gas. Below 300°C the product is a surface oxide, Ir_sO, but above 300°C numerous individual IrO_2 crystals are formed.

3. The formation of Ir_sO changes the original Pt-rich surface of alloy particles in favor of Ir, but the original surface composition can be restored by heating in H_2 at 400°C for 20 hr.

4. In the range 300–550°C, crystals of IrO_2 grow out of alloy particles and oxide and metal are in intimate contact. Above 550°C gas phase transport of IrO_2 leads to the formation of large oxide crystals separate from metal particles.

5. The reduction of IrO_2 is autocatalytic; hydrogen chemisorbs dissociatively on nucleated or residual metal particles and then diffuses in atomic form onto the adjacent oxide, where it facilitates the nucleation of further metal particles.

REFERENCES

1. Sinfelt, J. H., U.S. Patent 3,953,368 (1976).
2. (*a*) Sinfelt, J. H., and Via, G. H., *J. Catal.* **56,** 1 (1979); (*b*) Garten, R. L., and Sinfelt, J. H., *J. Catal.* **62,** 127 (1980).
3. Yates, D. J. C., and Kmak, W. S., U.S. Patent 3,937,660 (1976); U.S. Patent 3,943,052 (1976).
4. Wimber, R. T., and Kraus, H. G., *Metall. Trans.* **5,** 1565 (1974).
5. McVicker, G. B., Garten, R. L., and Baker, R. T. K., *J. Catal.* **54,** 129 (1978).
6. Foger, K., and Anderson, J. R., *J. Catal.* **54,** 318 (1978).

7. Klug, H. P., and Alexander, L. E., "X-Ray Diffraction Procedures for Polycrystalline and Amorphous Materials," pp. 372. Wiley, New York, 1974.
8. Rogers, D. B., Shannon, R. D., Sleight, A. W., and Gillson, J. L., *Inorg. Chem.* **8**, 841 (1969).
9. JCPDS "Powder Diffraction File," Swarthmore, Pa., File Nos. 23–1305, pp. 15–870.
10. Rasser, J. C., Beindorff, W. H., and Scholten, J. J. F., *J. Catal.* **59**, 211 (1979).
11. Raub, E., *J. Less-Common Metals* **1**, 3 (1959).
12. Carter, J. L., Cusumano, J. A., and Sinfelt, J. H., *J. Catal.* **20**, 223 (1971).
13. Williams, F. L., and Nason, D., *Surface Sci.* **45**, 377 (1974).
14. Kuijers, F. J., and Ponec, V., *Appl. Surface Sci.* **2**, 43 (1978).
15. Lee, J. B., unpublished results from this laboratory.
16. Raub, E., and Plate, W., *Z. Metallk.* **47**, 688 (1956).
17. Wagstaff, N., and Prins, R., *J. Catal.* **59**, 446 (1979).
18. Fiedorow, R. M. J., Chadar, B. S., and Wanke, S. E., *J. Catal.* **51**, 193 (1978).
19. Chen, M., and Schmidt, L. D., *J. Catal.* **55**, 348 (1978).
20. Krier, C. A., and Jaffee, R. I., *J. Less-Common Metals* **5**, 411 (1973).
21. Norman, J. H., Staley, H. C., and Bell, W. E., *J. Chem. Phys.* **42**, 1123 (1965).
22. Berkes, J. S., White, W. B., and Roy, R., *J. Appl. Phys.* **36**, 3276 (1965).
23. Foger, K., and Anderson, J. R., *J. Catal.* **59**, 325 (1979).
24. Brooks, C. S., *J. Colloid Interface Sci.* **34**, 419 (1970).
25. Maire, G., Hilaire, L., Legare, P., Gault, F. G., and O'Cinneide, A., *J. Catal.* **44**, 293 (1976).
26. Foger, K., and Jaeger, H., *J. Catal.*, **67**, 253 (1981).
27. Nowak, E. J., and Koros, R. M., *J. Catal.* **7**, 50 (1967).
28. Yao, H. C., Sieg, M., and Plummer, H. K., Jr., *J. Catal.* **59**, 365 (1979).